Entrainment of low Mach number thermals in stratified domains

Evan H. Anders,[1,2] Daniel Lecoanet,[3] and Benjamin P. Brown[1,2]

[1]*Dept. Astrophysical & Planetary Sciences, University of Colorado – Boulder, Boulder, CO 80309, USA*
[2]*Laboratory for Atmospheric and Space Physics, Boulder, CO 80303, USA*
[3]*Stuff*

ABSTRACT

Keywords: hydrodynamics — turbulence — entrainment

1. INTRODUCTION

Recent observations of solar convection have revealed a convective conundrum. Power spectra have revealed weaker flows than anticipated at large length scales, calling into question the existence of so-called "giant cells" driven by deep convection which would manifest as powerful, large-scale motions at the solar surface. This discrepancy between theory and observations has called into question our fundamental understanding of convection, sparking fruitful investigations into the nature of convection in the Sun.

Spruit (1997) hypothesized that convective motions may be driven entirely by cool downflows at the surface of the Sun, and Brandenburg (2016) expanded upon this "entropy rain" hypothesis. Brandenburg's work includes a careful expansion of mixing length theory to incorporate flux contributions from nonlocal convective motions, and handles this theory in a horizontally-averaged sense. He includes some discussion of possible flow morphologies which could be manifestations of this entropy rain, and even includes some brief simulations of propagating Hill vortices. However, these simulations and discussions did not include include a fundamental piece of entropy rain: it is buoyant, and has an entropy deviation from the background atmosphere.

If entropy rain does evolve into downward propagating buoyant vortex rings, it is important to understand how buoyancy effects the filling factor of these basic convective elements. In the context of Earth's atmosphere, so-called "thermals" are thought to be the nucleus of

Corresponding author: Evan H. Anders
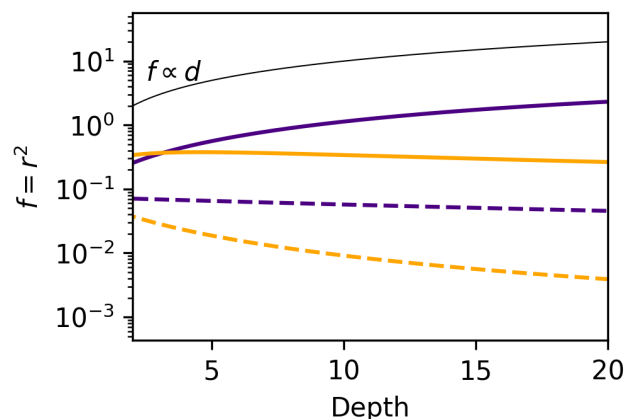evan.anders@colorado.edu

Figure 1.

cloud formation. Thermals are buoyant areas of fluid which evolve into propagating buoyant vortex rings, and their evolution in the Boussinesq limit have been well studied in the laboratory for decades (see e.g., CITE), and more recently have been studied through Direct Numerical Simulation (DNS) in the laminar and turbulent regime (Lecoanet & Jeevanjee 2018). One fundamental result of these studies of thermals is that they experience a large degree of entrainment: their size expands with height and their propagation velocity slows despite their buoyant nature. However, we do not know of a study in which the propagation of these thermals, and thus the nature of their entrainment, is affected by a significant atmospheric stratification.

In the absence of buoyantly-induced entrainment, Brandenburg (2016) suggests that the filling factor, f, of vortex rings should decrease like $f \propto \rho^\alpha$ for horizontal compression and $f \propto \rho^\alpha$ for spherical compression. On

the other hand, the filling factor of Boussinesq thermals *increases* like $f \propto d$, where d is the depth propagated. In this work, we extend the study of Lecoanet & Jeevanjee (2018) to study the propagation of low-Mach number, cold thermals in stratified domains, and how buoyant entrainment affects the scaling of their filling factor with depth. If buoyant entrainment is a dominant effect, it is possible that these buoyant vortex rings would simply grow too large and stall before reaching the bottom of the solar convection zone. On the other hand, if the compression effects suggested by Brandenburg (2016) are the dominant effect, then it is possible that these thermals could propagate to the bottom of the solar convection zone, or potentially shrink to a sufficiently small size where thermal dissipation is significant.

We lay out our work as follows. In section 2, we develop a theoretical description of thermals in a stratified domain. In section 3, we describe and verify the experiments conducted in this work. In section 4, we compare the results of our experiments to the theory developed in section 2. Finally, in section 5, we discuss what our results imply for the entropy rain hypothesis.

2. THEORY

2.1. *Phenomenological description of thermal evolution*

We show pictorally the evolution of a cold thermal from rest in Fig. 2. In Fig. 2a, the evolution of a thermal in a weakly stratified domain with $n_\rho = 0.5$ density scale heights is shown. In Fig. 2b, the evolution of a thermal in an appreciably stratified domain with $n_\rho = 3$ density scale heights is shown. While the initial conditions are identical in both domains (spherical specific entropy perturbations of the same magnitude whose diameters are 5% of the domain depth), and while in both cases the thermal quickly evolves into a propagating buoyant vortex ring, we find that the $n_\rho = 0.5$ case entrains and grows with depth, similarly to the Boussinesq regime. On the other hand, the $n_\rho = 3$ case has a radius which remains approximately constant over time, and it reaches the bottom of the domain in many fewer nondimensional freefall time units.

2.2. *Evolution of momentum and impulse*

The evolution of thermals as buoyant vortex rings has been well described in the unstratified, Boussinesq limit for decades (as early as e.g., CITE, and see Lecoanet & Jeevanjee (2018) for other sources). Buoyant motions in the atmospheres of stars and planets are generally large enough to feel the atmospheric stratification, and therefore a more thorough treatment of the evolution of thermals in stratified domains is required to understand thermal entrainment in nature. We will use a description
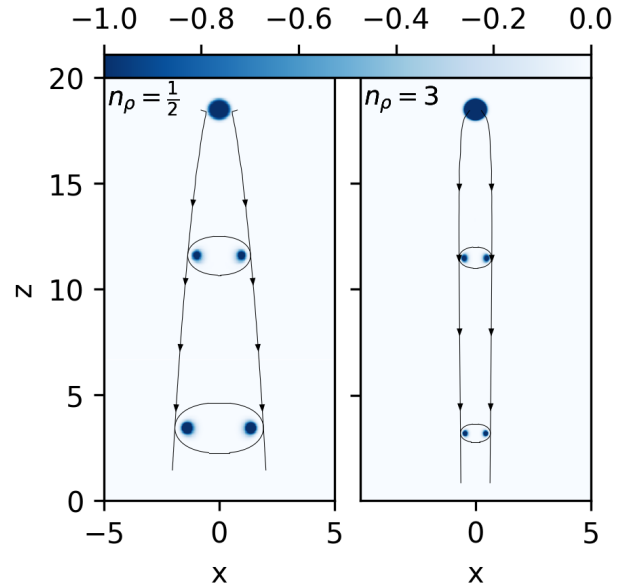

Figure 2.

of the momentum and impulse acting on the thermal to develop a theory of depth of thermals as a function of time, as well as the growth of their radii with depth.

In this work, we study an ideal gas and focus on the ideal, low Mach number regime in an adiabatically stratified atmosphere. In this regime, a linearized equation of state describes the thermodynamics well, and the fully compressible Euler momentum equation takes the form (Brown et al. 2012),

$$\frac{\partial \boldsymbol{u}}{\partial t} + \boldsymbol{u} \cdot \nabla \boldsymbol{u} = -\nabla \varpi - \frac{S_1}{c_P}\boldsymbol{g}, \tag{1}$$

where $\boldsymbol{u}$ is the velocity, $\varpi = P_1/\rho_0$ is the reduced pressure, $S = c_V \ln T - R \ln \rho$ is the specific entropy, and thermodynamics are broken down into background (subscript 0) and fluctuating (subscript 1) components. In this work we find it instructive to examine the full momentum, and so multiplying this equation by the density, we obtain,

$$\frac{\partial(\rho\boldsymbol{u})}{\partial t} + \boldsymbol{u} \cdot \nabla(\rho\boldsymbol{u}) + \rho\boldsymbol{u}(\nabla \cdot \boldsymbol{u}) = -\rho\nabla\varpi - \rho\frac{S_1}{c_P}\boldsymbol{g}. \tag{2}$$

Hereafter we will define the Lagrangian derivative, $D/Dt \equiv \partial/\partial t + \boldsymbol{u} \cdot \nabla$, and we acknowledge that the Langrangian derivative commutes with a volume integral such that

$$\frac{D}{Dt}\int_{\mathcal{V}} f\, dV = \int_{\mathcal{V}}\left[\frac{Df}{Dt} + f(\nabla \cdot \boldsymbol{u})\right] dV.$$

Volume-integrating Eqn. 2, we thus find

$$\frac{D\boldsymbol{M}}{Dt} = \int_{\mathcal{V}}\left(-\rho\nabla\varpi - \rho\frac{S_1}{c_P}\boldsymbol{g}\right) dV, \tag{3}$$

where the volume-integrated momentum is defined $M \equiv \int_{\mathcal{V}} \rho u dV$. At this point we will make the assumption of a plane-parallel atmosphere in which the gravity is constant, $g = -g\hat{z}$, and note that the z-component of the volume-integrated momentum evolves according to

$$\frac{DM_z}{Dt} = \int_{\mathcal{V}} \left(-\rho \frac{\partial \varpi}{\partial z} + \rho g \frac{S_1}{c_P} \right) dV. \tag{4}$$

At this point, we find it useful to define the total buoyancy,

$$B \equiv \int_{\mathcal{V}} \rho S_1 \frac{g}{c_P} dV, \tag{5}$$

as in the absence of viscosity and detrainment, this is a conserved quantity during thermal evolution (REFERENCE FIGURE). Furthermore, in the Boussinesq limit, the work of Tarshish et al. (2018) shows that pressure terms reduce the efficacy of the buoyancy in changing the momentum by effectively reducing the buoyant acceleration by some factor $\beta \sim 0.5$. As a result, we can approximate the growth of a thermal's momentum according to

$$\frac{DM_z}{Dt} \approx \beta B. \tag{6}$$

After describing the growth of the thermal's integrated momentum with time, we turn our attention to th ehydrodynamic impulse, which in the stratified limit is defined (Shivamoggi 2010),

$$I = \frac{1}{2} \int_{\mathcal{V}} x \times (\nabla \times (\rho u)) dV, \tag{7}$$

where x is the position vector. Impulse is equivalent to the time-integrated work acting on the fluid resulting in the current fluid motion. Per Shivamoggi (2010), changes in the impulse can be expressed as

$$\frac{DI}{Dt} = \int_{\mathcal{V}} \frac{\partial(\rho u)}{\partial t} dV = B\hat{z} - \int_{\mathcal{V}} [\rho \nabla \varpi + \nabla \cdot (\rho u u)] dV,$$

where, importantly, the *eulerian* derivative of the momentum is inside of the volume integral here. Under the proper specification of boundary conditions, the integral term is zero, and the vertical impulse of a thermal thus straightforwardly changes in time as

$$\frac{DI_z}{Dt} = B. \tag{8}$$

We have thus retrieved the two findings on which our theory of thermal evolution will be built: *both the impulse and momentum experience constant changes in time determined by the buoyant nature of the thermal.*
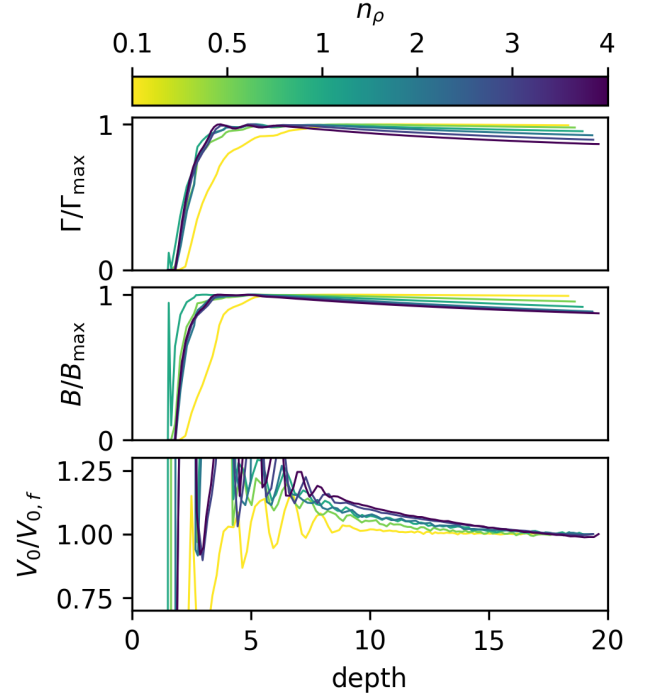

Figure 3.

2.3. *Parameterized description of thermal evolution*

We first note, as in Fig. 3a, that the buoyancy in our thermals is not necessarily perfectly constant in time, and that effects like detrainment result in a minor reduction of the buoyant signature of our thermals. We thus express the buoyancy in terms of two constants,

$$B \approx \chi B_0, \tag{9}$$

where B_0 is the initial buoyancy of the thermal, and χ is a constant of O(1) which represents this detrainment. We then integrating Eqn. 8 in time,

$$I_z = \chi B_0 t + I_0.$$

In the low-Mach number limit in which changes in density from the background are negligible, the impulse of a vortex ring can be approximated as

$$I_z \approx \pi \rho r^2 \Gamma_0,$$

where r is the radius of the thermal from its axis of symmetry to the maxima of its buoyant signature, and $\Gamma_0 = \int_{\mathcal{A}} (\nabla \times u) dA$ is the integrated circulation in a cross-section of the vortex ring. We take Γ_0 to be constant, which is a decent assumption in our experiments, see Fig. 3b. Combining these two expressions, we retrieve our first result,

$$r = \sqrt{\frac{\chi B_0 t + I_0}{\pi \rho \Gamma_0}}. \tag{10}$$

In the Boussinesq limit where $\rho \rightarrow$ constant, we retrieve the $r \propto \sqrt{t}$ scaling found in the Boussinesq regime by Lecoanet & Jeevanjee (2018). We find that the inclusion of stratification adds the additional complexity of $r \propto \rho^{-1/2}$, such that downward-propagating vortex rings (as studied here) will entrain less than boussinesq thermals, and upward-propagating rings will entrain more. In the absence of buoyancy ($B = 0$), this result aligns with the prediction for purely horizontal compression noted by Brandenburg (2016) of $r^2 \propto \rho^{-1}$.

The momentum can likewise be integrated like the impulse,

$$M_z = \beta \chi B_0 t + M_0.$$

For the proper choice of vertical velocity, w_{th}, and volume, $\mathcal{V}$, the momentum can be expressed precisely as

$$M_z = \rho \mathcal{V} w_{\mathrm{th}},$$

and the volume can be approximated as $\mathcal{V} = f r^3$, where f is a parameter which we take to be constant. This assumption is perhaps not as perfect as the assumptions of constant B_0 or Γ_0 (see Fig. 3c), but it is nevertheless not a bad assumption. Combining our approximate expressions, and inserting our theoretical description of r (Eqn. 10), we retrieve

$$\rho^{-1/2} w_{\mathrm{th}} = \left(\frac{(\pi\Gamma)^{3/2}}{f} \right) \frac{\beta \chi B_0 t + M_0}{(\chi B_0 t + I_0)^{3/2}}. \tag{11}$$

Defining the thermal velocity $w_{\mathrm{th}} \equiv dz_{\mathrm{th}}/dt$, and making the assumption that the vortex ring starts at a "virtual origin" (CITE) at $t = 0$ where it has no impulse or momentum ($I_0 = M_0 = 0$), an integrable expression for the evolution of thermal position over time can be retrieved,

$$\frac{dz_{\mathrm{th}}}{\rho (z_{\mathrm{th}})^{1/2}} = \left(\frac{\beta (\pi\Gamma)^{3/2}}{f (\chi B_0)^{1/2}} \right) \frac{dt}{t^{1/2}} \tag{12}$$

If the atmospheric stratification in which the thermal is falling is known, this result can be integrated with $\rho(z_{\mathrm{th}})$ plugged in in order to find the position of the thermal as a function of time. We leave this result general for now, and will integrate it using the polytropic stratification used in our simulations at the end of section 3.

3. EXPERIMENT

3.1. *Anelastic Simulations*

In this work, we primarily study the evolution of 2D, azimuthally symmetric, anelastic thermals in cylindrical coordinates. We later verify that select simulations produce the same results as 3D fully compressible simulations in cartesian domains (see sec. REF). The LBR

anelastic equations are (Lecoanet et al. 2014),

$$\widetilde{\nabla} \cdot \widetilde{\boldsymbol{u}} = -\widetilde{w} \partial_{\tilde{z}} \ln \rho_0 \tag{13}$$

$$\frac{D\widetilde{\boldsymbol{u}}}{D\widetilde{t}} = -\widetilde{\nabla}\widetilde{\varpi} + g\frac{\widetilde{S_1}}{c_P}\hat{z} + \frac{1}{\rho_0}\widetilde{\nabla} \cdot \left(\mu \widetilde{\bar{\bar{\boldsymbol{\sigma}}}} \right) \tag{14}$$

$$\frac{D\widetilde{S_1}}{D\widetilde{t}} = \frac{1}{\rho c_P}\widetilde{\nabla} \cdot \left(\kappa T_0 \widetilde{\nabla}\widetilde{S_1} \right) + \frac{\mu}{\rho_0 T_0}\widetilde{\sigma}_{ij}\partial_{\tilde{x}_i}\widetilde{u}_j. \tag{15}$$

where terms with tildes are dimensional, and where $D/D\widetilde{t} = \partial/\partial\widetilde{t} + \widetilde{\boldsymbol{u}} \cdot \widetilde{\nabla}$. In our azimuthally symetric domain, we assume that $\partial_\phi = 0$; as the initial conditions of our simulations are at rest and have no azimuthal velocity, u_ϕ, we explicitly impose that $u_\phi = 0$; therefore $\boldsymbol{u} = u_r\hat{r} + w\hat{z}$. Under this approximation, the components of the stress tensor are

$$\widetilde{\sigma}_{rr} = 2\frac{\partial\widetilde{u_r}}{\partial\widetilde{r}} - \frac{2}{3}\widetilde{\nabla} \cdot \widetilde{\boldsymbol{u}}, \quad \widetilde{\sigma}_{\phi\phi} = 2\frac{\widetilde{u_r}}{\widetilde{r}} - \frac{2}{3}\widetilde{\nabla} \cdot \widetilde{\boldsymbol{u}},$$
$$\widetilde{\sigma}_{zz} = 2\frac{\partial\widetilde{w}}{\partial\widetilde{z}} - \frac{2}{3}\widetilde{\nabla} \cdot \widetilde{\boldsymbol{u}}, \quad \widetilde{\sigma}_{rz} = \widetilde{\sigma}_{zr} = \frac{\partial\widetilde{w}}{\partial\widetilde{r}} + \frac{\partial\widetilde{u_r}}{\partial\widetilde{z}}, \tag{16}$$
$$\widetilde{\sigma}_{r\phi} = \widetilde{\sigma}_{\phi r} = \widetilde{\sigma}_{\phi z} = \widetilde{\sigma}_{z\phi} = 0,$$

Furthermore, we assume that the dynamic viscosity, $\mu = \rho_0\nu$, and the thermal conductivity, $\kappa = \rho_0\chi$, are both uniform throughout the domain and constant in time. The diffusivities ν and χ therefore scale inversely with the density.

We nondimensionalize these equations in the same manner as in Lecoanet & Jeevanjee (2018) such that the length scale is the diameter of the initial thermal perturbation and the velocity scale is the freefall velocity. The timescale is thus the freefall crossing time of this unit length. Mathematically,

$$\widetilde{\nabla} \rightarrow (\widetilde{L}_{th}^{-1})\nabla, \qquad \widetilde{S_1} \rightarrow (\Delta\widetilde{S})S_1,$$
$$\widetilde{\boldsymbol{u}} \rightarrow (\widetilde{u}_{th})\boldsymbol{u}, \qquad \widetilde{\varpi} \rightarrow (\widetilde{u}_{th}^2)\varpi, \tag{17}$$
$$\partial_{\tilde{t}} \rightarrow (\widetilde{u}_{th}/\widetilde{L}_{th})\partial_t,$$

with

$$\tilde{u}_{th}^2 = \frac{g\tilde{L}_{th}\Delta\tilde{s}}{c_P}, \qquad \mathrm{Re}_{\mathrm{ff}} = \frac{\tilde{u}_{th}\tilde{L}_{th}}{\nu}, \qquad \mathrm{Pr}_{\mathrm{ff}} = \frac{\tilde{u}_{th}\tilde{L}_{th}}{\chi}. \tag{18}$$

As the diffusivities scale with depth, $\mathrm{Re_{ff}}$ is specified at the thermal's initial depth. The resulting equations are,

$$\nabla \cdot \boldsymbol{u} = -w\partial_z \ln \rho_0, \qquad (19)$$

$$\partial_t \boldsymbol{u} + \boldsymbol{u} \cdot \nabla \boldsymbol{u} =$$
$$-\nabla \varpi + S_1 \hat{z} + \frac{1}{\mathrm{Re_{ff}}} \left[\nabla^2 \boldsymbol{u} + \frac{1}{3} \nabla (\nabla \cdot \boldsymbol{u}) \right] \qquad (20)$$

$$\partial_t S_1 + \boldsymbol{u} \cdot \nabla S_1 =$$
$$\frac{1}{\mathrm{Re_{ff}}} \left(\frac{1}{\mathrm{Pr_{ff}} \rho_0 c_P} [\nabla^2 S_1 + \partial_z \ln T_0 \cdot \partial_z S_1] \right. \qquad (21)$$
$$\left. + \frac{-(\nabla_{\mathrm{ad}})}{\rho_0 T_0} \sigma_{ij} \partial_{x_i} u_j \right),$$

where $\nabla_{\mathrm{ad}} \equiv \tilde{L}_{\mathrm{th}} \frac{g}{c_P}$.

3.2. *Atmosphere & Initial conditions*

We study an ideal gas whose equation of state is $P = \rho T$ and whose stratification is a perfectly adiabatic polytrope,

$$T_0 = 1 + (\nabla_{\mathrm{ad}})(z - L_z) \qquad (22)$$
$$\rho_0 = T_0^{m_{\mathrm{ad}}}, \qquad (23)$$

where $m_{\mathrm{ad}} = (\gamma - 1)^{-1}$, and the adiabatic temperature gradient in these nondimensional atmospheres is set with $g = m_{\mathrm{ad}} + 1$ and $\tilde{L}_{\mathrm{th}} = (e^{n_\rho/m_{\mathrm{ad}}} - 1)/L_z$, where n_ρ is the number of density scale heights spanned by the atmosphere and $L_z = 20$ is the nondimensional depth of the atmosphere in units of thermal diameters.

To initialize the simulation, we specify a spherical initial specific entropy perturbation,

$$S_1 = -\frac{A}{2} \left[1 - \mathrm{erf}\left(\frac{r' - r_{th}}{\delta} \right) \right], \qquad (24)$$

where $A = 1$ for our scaled equations. Here, $r' = \sqrt{r^2 + (z - z_0)^2}$, where $z_0 = L_z - 3r_{\mathrm{th}}$, with the thermal radius set as $r_{th} = 0.5$, and a smoothing width, $\delta = 0.1$.

3.3. *Fully Compressible Simulations*

In order to verify the validity of our 2D Anelastic simulations, we evolve select thermals according to the 3D Navier Stokes equations in a cartesian domain. We use the $(T, \ln \rho)$ formulation of the equations in which we have previously studied fully compressible convection at low and high Mach number (Lecoanet et al. 2014; Anders & Brown 2017),

$$\frac{D \ln \rho}{Dt} + \nabla \cdot \boldsymbol{u} = 0 \qquad (25)$$

$$\frac{D\boldsymbol{u}}{Dt} = -\nabla T - T \nabla \ln \rho - g\hat{z} + \frac{1}{\rho} \nabla \cdot (\mu \bar{\bar{\boldsymbol{\sigma}}}) \qquad (26)$$

$$\frac{DT}{Dt} + (\gamma - 1) T \nabla \cdot \boldsymbol{u} = \frac{1}{\rho c_V} \nabla \cdot (\kappa \nabla T) + \frac{\mu}{\rho c_V} \sigma_{ij} \partial_{x_i} u_j. \qquad (27)$$

where the viscous stress tensor is defined as

$$\sigma_{ij} = \left(\partial_{x_i} u_j + \partial_{x_j} u_i - \frac{2}{3} \delta_{ij} \nabla \cdot \boldsymbol{u} \right). \qquad (28)$$

These equations are nondimensionalized on the temperature gradient length scale such that $\nabla_{\mathrm{ad}} = -1$ and the nondimensional timescale is the sound crossing time of that unit length at the top of the domain.

In setting the specific entropy, $S = c_V \ln T - R^{-1} \ln \rho$, to an equivalent condition to that specified in Eqn. 24, we note that it is essential that the initial perturbation be in pressure equilibrium. The set of initial conditions that achieves this is

$$\ln \rho_1 = S_1/c_P, \qquad T_1 = T_0(e^{-\ln \rho_1} - 1). \qquad (29)$$

We specify the magnitude of the initial entropy perturbations as $A = \epsilon = 10^{-4}$, such that the mach number of the resultant thermal is $\mathrm{O}(10^{-2})$ or less.

The depth of the atmosphere in these fully compressible domains is set to $L_z = e^{n_\rho/m_{\mathrm{ad}}} - 1$. In order to compare results from these simulations to our Anelastic thermal simulations, we rescale all outputs in postprocessing by a length scale factor of $\ell = 20/L_z$, a timescales factor of $\tau = \sqrt{\ell}\epsilon$, and a specific entropy scaling of $s = \epsilon^{-1}$.

3.4. *Numerics*

We evolve our simulations forward in time using the Dedalus[1] pseudospectral framework (Burns et al. 2016) to time-evolve our equations. For our 2D simulations, we use using an implicit-explicit (IMEX), third-order, four-stage Runge-Kutta timestepping scheme RK443 (Ascher et al. 1997), and for our 3D simulations we use the second order semi-implicit backward differentiation formulation SBDF2 (Wang & Ruuth 2008).

Our 3D simulations are decomposed on Fourier bases in the horizontal directions $(x, y \in [-L_r, L_r])$ and Chebyshev bases vertically $(z \in [0, L_z])$ with impenetrable, stress free, fixed-temperature boundary conditions at the upper and lower boundaries $(T_1 = w = \partial_z u = \partial_z v = 0$ at $z = [0, L_z])$. Our 2D simulations are decomposed on a Fourier $(z \in [0, L_z])$ and Chebyshev $(r \in [0, L_r])$ domain, with boundary conditions of $\partial_r S_1 = w = (\nabla \times \boldsymbol{u})_\phi = 0$ at $r = L_r$.

3.5. *Solution for thermal evolution in a Polytrope*

Now that the atmospheric density is specific, we can find an explicit solution for Eqn. 12 to compare to the results of our simulations. As temperature and height are

---

[1] http://dedalus-project.org/

linearly related in our atmospheres, we find it instructive to use temperature as a integration parameter. We note that, $\rho = T^{m_{ad}}$ and $dT = (\nabla_{\rm ad})dz_{th}$, such that we must solve

$$\int_{T_0}^{T_{\rm th}} T^{-m_{ad}/2}dT = \left(\frac{\beta(\pi\Gamma)^{3/2}\nabla_{\rm ad}}{f(\chi B)^{1/2}}\right)\int_0^{t+t_{\rm off}} t^{-1/2}dt.$$
(30)

defining $C \equiv \beta\pi^{3/2}\nabla_{\rm ad}/f\sqrt{\Gamma^3/(\chi B)}$ and $\alpha^{-1} = 1 - m_{\rm ad}/2$, and ssuming that $m_{\rm ad} < 2$ (which is valid for our case of $m_{\rm ad} = 1.5$ studied here) we find that

$$T_{\rm th} = \left(\frac{2C}{\alpha}\sqrt{t + t_{\rm off}} + T_0^{1/\alpha}\right)^{\alpha}.$$
(31)

In the limit of large stratification, we thus find that $T_{\rm th} \propto t^2$ for our case of $\alpha = 4$. The temperature can be straightforwardly converted to height by a rearrangement of Eqn. 23,

$$z_{\rm th} = (T_{\rm th} - 1)/\nabla_{\rm ad} + L_z$$
(32)

The thermal is thus described in terms of seven total parameters:

1. T_0 and $t_{\rm off}$, the temperature of the thermal's virtual origin, and the time before the simulation's $t = 0$ at which the thermal was located at its virtual origin,

2. B_0 and Γ, the measurable buoyancy and circulation of the vortex ring, and

3. f, χ, and β, fitting parameters which describe the nature of the vortex ring's evolution.

The measured values of these parameters for the cases studied in this paper are presented in table 1.

4. RESULTS

In Fig. 4, we show the measured depth $d_{\rm th} = L_z - z_{\rm th}$ of the thermal as a function of time for low and high stratification. At very low stratification (e.g., $n_\rho = 0.1$), the thermal is small compared to the local density scale height at all depths, and it evolves roughly according to the Boussinesq prediction of $d \propto \sqrt{t}$. As the stratification increases, the thermal begins to transit the domain more quickly and approaches the limit of $d \propto t^2$ predicted in the highly stratified limit of Eqn. 31. The theoretical fits for depth from the prediction of Eqn. 31 are plotted over the measured data and show remarkable agreement.

In Fig. 5a, we plot the measured thermal radius vs. depth, with the theoretical predictions of Eqns. 10 & 31 plotted as lines over the data. In the low stratification limit, the radius of the thermal grows linearly with
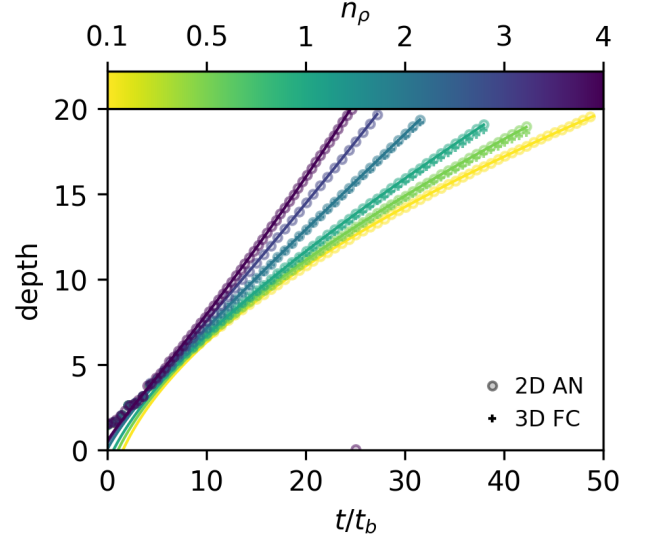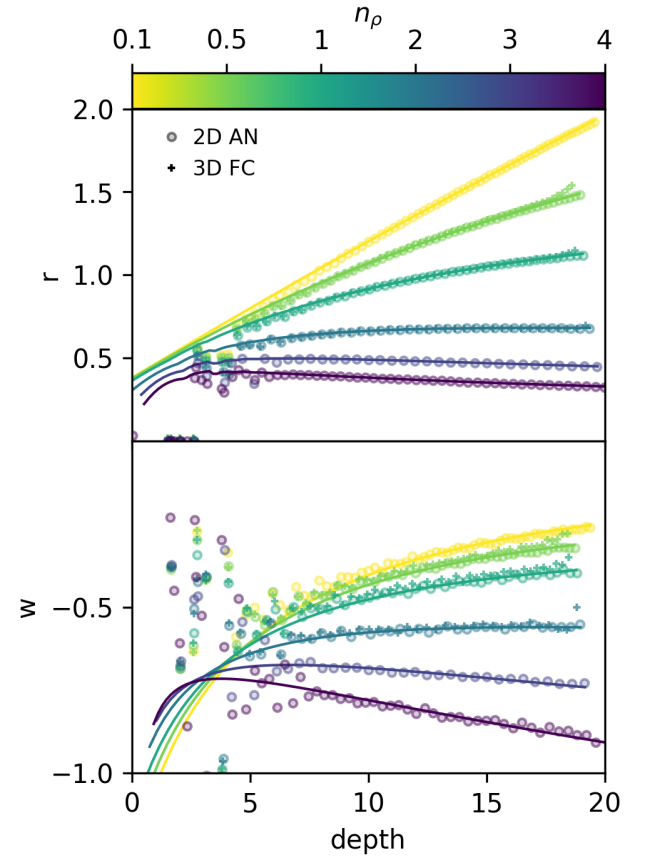

Figure 4.

Figure 5.

depth, $r \propto d$, aligning with the Boussinesq limit shown in Lecoanet & Jeevanjee (2018) This growth of the thermal is the result of entrainment of environmental fluid

Table 1. Simulation output parameterization

n_ρ	∇_{ad}	T_0	t_{off}	B	Γ	f	χ	β
2D Anelastic Simulations								
0.1	3.45×10^{-3}	0.985	0.166	-0.547	-2.17	7.01	1.04	0.499
0.5	1.98×10^{-2}	0.918	0.704	-0.568	-2.12	7.04	0.976	0.490
1	4.74×10^{-2}	0.827	1.09	-0.601	-2.05	7.07	0.915	0.480
2	0.140	0.677	1.26	-0.712	-1.89	7.08	0.841	0.456
3	0.319	0.619	1.01	-0.946	-1.73	7.08	0.808	0.436
4	0.667	0.698	0.622	-1.47	-1.59	7.10	0.793	0.422
5	1.352							
3D Fully Compressible Simulations								
0.5	1.98×10^{-2}	0.924	0.583	-0.568	-2.12	6.66	0.978	0.452
1	4.74×10^{-2}	0.832	1.26	-0.601	-2.05	6.88	0.902	0.454
2	0.140	0.666	1.53	-0.711	-1.89	7.08	0.822	0.450

NOTE— Values from fully compressible simulations have been rescaled in post-processing for direct comparison with 2D anelastic cases

and results an an accompany decceleration like $w \propto d^{-1}$ in the Boussinesq limit, as is shown in Fig. 5b. However, as stratification increases, the thermal entrains less environmental fluid and expands less, eventually even contracting with depth in the high-stratification limit. This lessened entrainment is, unsurprisingly, accompanied by greater acceleration of the thermal. As in the case of depth vs. time, the overplotted theoretical predictions show excellent agreement with the measured data.

These results suggest that there are two regimes of downflowing thermal behavior:

1. A low-stratification "stalling" regime, in which the thermal entrains environmental fluid and slows down, acting much like the Boussinesq regime, and

2. A high-stratification "falling" regime, in which the thermal falls fast enough that compression due to the atmospheric stratification results in minimal entrainment and the thermal accelerates as it falls deeper into the atmosphere.

However, we note that both of these regimes could result in interesting problems for the entropy rain hypothesis. If solar convection were comprised of thermals in the stalling regime, it is unlikely that such elements would ever make it to the base of the solar convection zone, stalling much closer to the solar surface and depositing their entropy signature there – possibly agreeing with the hypothesis of supergranulation as the largest buoyantly driven scale of solar motion. On the other hand, if solar convection is comprised of thermals in the falling regime, then it is possible that as these thermals compress and accelerate, diffusive effects and potentially viscous heating could become important. We discuss these possibilities further in section 5

4.1. *Verification of 2D Anelastic approximation*

In Fig. 6, we display in more detail a comparison of our 2D Anelastic and 3D Fully Compressible cases. In Fig. 6a, depth vs time is shown, and the fractional difference between FC and AN cases is shown in Fig. 6b. Differences between the two cases are $\leq 2\%$ for all times, with greater error towards the end of the simulations as the FC simulations begin to interact with the impenetrable boundary at the bottom of their simulation domains. In Fig. 6c, radius vs. depth is shown, and the fractional difference between FC and AN cases is shown in Fig. 6d. Aside from the very end of the simulation when the FC boundary conditions begin to matter, there is remarkable agreement between the two cases, with $< 1\%$ differences between the two cases after early times in which the thermal is still developing into a vortex ring.

This close agreement between low Mach number Fully Compressible simulations and Anelastic simulations parallels the agreement between the equation sets seen in Lecoanet et al. (2014), and gives us confidence in our anelastic results at higher levels of stratification, where the 2D simulations are much more numerically feasible than the 3D fully compressible simulations.

5. DISCUSSION

In this work we have extended the theory of the evolution of buoyant thermals into the low-Mach number, stratified regime and have shown that that theory has remarkable agreement with the results of both Anelastic and Fully compressible simulations.

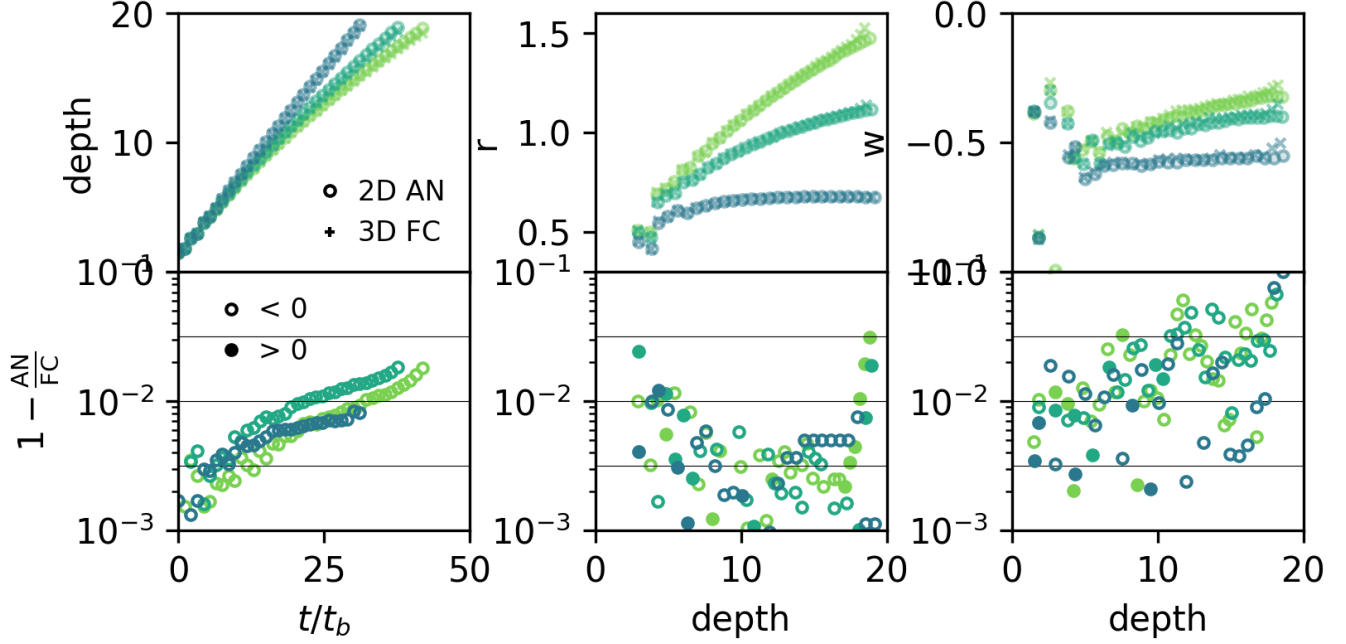We should have some discussion on these topics:

Figure 6.

1. speculation about extensions to the solar regime. Do things on the sun shrink to the point where they viscously dissipate? Do they stall?

2. Talk about what would happen if we were to study up-thermals.

3. Extensions, and we trust that these results should hold in the regime of solar convection where things are turbulent.

APPENDIX

A. THERMAL TRACKING

We use a thermal tracking algorithm very similar to the one used in Lecoanet & Jeevanjee (2018) and inspired by the work of Romps & Charn (2015).

We begin by measuring the thermal's height versus time. To do so, we average the domain's entropy profile in radius and azimuth to create an average profile of entropy with height, and then assume that the thermal's vortex core is located at the entropy minima of each of those profiles. We numerically differentiate these found values of height vs. time using (insert numerical differentiation technique here) and then calculate the streamfunction of the velocity field as in Romps & Charn (2015),

$$\frac{\partial \psi}{\partial r} = 2\pi \rho r (w - w_{\text{th}}), \tag{A1}$$

with the boundary condition that $\psi = 0$ at $r = 0$. The contour defined by $\psi = 0$ from this solution is taken to be the outline of the thermal, and the volume of the thermal is taken to be the volume radially inward from that contour.

Table 2. Table of simulation information

n_ρ	$L_{thermal}/H_\rho$	nr or nx = ny	nz	$t_{evolution}$	safety
2D Anelastic Simulations					
0.1		256	512	49	0.2
0.5		256	512	42.5	0.2
1		256	512	38	0.2
2		256	512	31.75	0.2
3		512	1024	27.25	0.2
4		1024	1024	25	0.2
5					
6					
7					
3D Fully Compressible Simulations					
0.5		256	512	45	0.2
1		256	512	45	0.2
2		256	1024	45	0.2
3		256	2048	45	0.2

Note—

B. TABLE OF SIMULATIONS

REFERENCES

Anders, E. H., & Brown, B. P. 2017, Physical Review Fluids, 2, 083501

Ascher, U. M., Ruuth, S. J., & Spiteri, R. J. 1997, Applied Numerical Mathematics, 25, 151

Brandenburg, A. 2016, ApJ, 832, 6

Brown, B. P., Vasil, G. M., & Zweibel, E. G. 2012, ApJ, 756, 109

Burns, K., Vasil, G., Oishi, J., Lecoanet, D., & Brown, B. 2016, Dedalus: Flexible framework for spectrally solving differential equations, Astrophysics Source Code Library, , , ascl:1603.015

Lecoanet, D., Brown, B. P., Zweibel, E. G., et al. 2014, ApJ, 797, 94

Lecoanet, D., & Jeevanjee, N. 2018, arXiv e-prints, arXiv:1804.09326

Romps, D. M., & Charn, A. B. 2015, Journal of Atmospheric Sciences, 72, 2890

Shivamoggi, B. K. 2010, Physics Letters A, 374, 4736

Spruit, H. C. 1997, Mem. Soc. Astron. Italiana, 68, 397

Tarshish, N., Jeevanjee, N., & Lecoanet, D. 2018, Journal of Atmospheric Sciences, 75, 3233

Wang, D., & Ruuth, S. J. 2008, Journal of Computational Mathematics, 26, 838